Lyapunov modes in three-dimensional Lennard-Jones fluids

2008 J. Phys. A: Math. Theor. 41 375101

(http://iopscience.iop.org/1751-8121/41/37/375101)

IOP PUBLISHING JOURNAL OF PHYSICS A: MATHEMATICAL AND THEORETICAL

J. Phys. A: Math. Theor. **41** (2008) 375101 (21pp) doi:10.1088/1751-8113/41/37/375101

Lyapunov modes in three-dimensional Lennard-Jones fluids

M Romero-Bastida[1,2] **and E Braun**[2]

[1] Facultad de Ciencias, Universidad Autónoma del Estado de Morelos, Avenida Universidad 1001, Chamilpa, Cuernavaca, Morelos 62209, México
[2] Departamento de Física, Universidad Autónoma Metropolitana Iztapalapa, Apartado Postal 55-534, Distrito Federal 09340, México

E-mail: rbm@xanum.uam.mx

Received 7 January 2008, in final form 15 July 2008
Published 7 August 2008
Online at stacks.iop.org/JPhysA/41/375101

Abstract

Recent studies on the phase-space dynamics of a one-dimensional Lennard-Jones fluid reveal the existence of regular collective perturbations associated with the smallest positive Lyapunov exponents of the system, called hydrodynamic Lyapunov modes, which previously could only be identified in hard-core fluids. In this work we present a systematic study of the Lyapunov exponents and Lyapunov vectors, i.e. perturbations along each direction of phase space, of a three-dimensional Lennard-Jones fluid. By performing the Fourier transform of the spatial density of the coordinate part of the Lyapunov vector components and then time-averaging this result we find convincing signatures of longitudinal modes, with inconclusive evidence of transverse modes for all studied densities. Furthermore, the longitudinal modes can be more clearly identified for the higher density values. Thus, according to our results, the mixing of modes induced by both the dynamics and the dimensionality induces a hitherto unknown type of order in the tangent space of the model herein studied at high density values.

PACS numbers: 05.45.Jn, 05.45.Pq, 02.70.Ns

1. Introduction

In recent years it has been possible to study in detail the underlying chaotic dynamics of many-particle systems, thus finding interesting connections between their microscopic dynamics and the observed macroscopic behavior. For example, in the case of static properties, the largest Lyapunov exponent (LLE), which measures the dynamical instability of phase-space trajectories to infinitesimal perturbations of the initial conditions, is related to

the Kosterlitz–Thoules transition temperature in a system of coupled rotators with nearest-neighbor interactions [1], as well as to first- [2] and second-order phase transitions [3] in particle systems with long-range interactions. For dynamical properties, the sudden change in the gradient of the LLE against energy, which corresponds to the transition from weak to strong chaos, can be detected in the macroscopic behavior of a Brownian particle coupled to the system [4]. It has also been related to transport coefficients of fluid systems with continuous potentials in non-equilibrium situations [5]. In equilibrium, a relation has also been proposed [6], although for this case arguments both against [7] and in favor [8] have been advanced. Nevertheless, these last results entail interesting possibilities, since they suggest that dynamical instability is at the origin of macroscopic transport phenomena. Two different methodologies have related the Lyapunov spectrum (LS), defined as the sorted set of Lyapunov exponents (LEs) which give the exponential rate of expansion or contraction of nearby trajectories along each independent component of the phase space, to the transport coefficients of simple fluids [9, 10]. However, they involve setting up non-equilibrium simulations or locating special phase-space trajectories. Furthermore, neither of these approaches considers the perturbations in phase space underlying the LEs, which have attracted a lot of attention in recent years. Therefore, it would be desirable first to attain a more thorough understanding of the phase-space perturbations associated with the LEs of the most general type of dynamical models employed to study fluid systems before attempting the construction of a general theory that could relate, with enough confidence, the dynamical instability to the macroscopic behavior as described by the transport coefficients.

For some particular many-particle systems, e.g. hard-sphere fluids, the theory of LEs is highly developed [11]. Nevertheless, their most interesting features have been discovered by means of molecular dynamics simulations, which revealed that the slowly-growing and decaying perturbations associated with the non-vanishing LEs closest to zero are related to, and in some cases may even be represented as, almost exact periodic vector fields coherently spread out over the physical space with well-defined wave vectors, together with an almost precise stepwise structure of the considered LEs [12]. From their similarity to the classical modes of fluctuating hydrodynamics, these perturbations have been named *Lyapunov modes* (LMs). Since their discovery [13], much work has been done to understand their origin and possible relevance. Some analytical approaches that have been advanced to understand these small LEs include random-matrix dynamics [14, 15], periodic orbit models [16] and kinetic theory [17, 18]. All these approaches have met with only a very limited success, since none of them has been able to satisfactorily describe the mode dynamics in all the known situations accessible to simulations. A more serious drawback is that neither has been capable of extracting the transport coefficients from the LMs, or of relating them, in a simple way, to hydrodynamic fluctuations.

Until recently the existence of these LMs could only be verified in one, two and three-dimensional hard-sphere fluids [13]; their existence in the case of atomic fluids with soft interactions (both attractive and repulsive) remained controversial [19], since certain features, such as the step structure in the LS, disappear in soft-potential systems. Hence, to extend the concept of LMs beyond the realm of hard-core systems, a more generic definition has to be adopted, which involves both the appearance of a sharp peak of low wave number in the spatial Fourier spectrum of LVs corresponding to the LEs closest to zero and of a minimum in the average spectral entropy, defined in section 4.2 of the present work, in that same LE region. Employing this more generic definition convincing evidence of the existence of the so-defined LMs was obtained for some soft-potential systems, namely in fluids with a one-dimensional (1D) Lennard-Jones (LJ) [20], where the aforementioned definition of LMs and the spectral analysis techniques needed to detect them were developed, and two-dimensional (2D)

Weeks–Chandler–Anderson (WCA) interaction potentials [21]. More recently, the existence of LMs has also been verified in lattices of coupled Hamiltonian and dissipative maps [22–24], as well as in Fermi–Pasta–Ulam anharmonic oscillator lattices [25]. Thus all information so far available seems to indicate that the Hamiltonian structure, conservation laws and translational invariance are not necessary conditions for the existence of LMs. Nevertheless, since there is no theoretical scheme that can predict the existence of LMs, the discovery and characterization of LMs has to be done in a case-by-case basis. For example, the introduction of damping in a system of coupled Hamiltonian maps does not destroy the LMs, whereas the addition of that same damping to a system of coupled circle maps wipes off the LMs [23]. Therefore, although LMs are present in the aforementioned systems, their existence is in no way guaranteed in other situations not studied so far, such as in three-dimensional Hamiltonian fluid systems with both attractive and repulsive interactions.

In this paper we perform a study of the dynamical instabilities of a three-dimensional (3D) atomic fluid interacting with the full LJ potential under the simulation conditions most frequently encountered in molecular dynamics studies [26]. We assess the validity of various dynamical indicators previously proposed in the literature for our particular system. The main result of our work is that, although the spectral analysis methods proposed in [20] can be readily applied to our system, the dimensionality greatly enhances the mixing among perturbations that was already present in the case of the 1D LJ gas, thus rendering both the detection and characterization of the collective perturbations even more problematic.

This paper is organized as follows: in section 2 we present a survey of the model, as well as the computational details needed to obtain our results in the phase space of our system as well as a short account of the relevant theory necessary to study the perturbations of the phase space. Section 3 describes the results for the complete LS, its dependence on the particle density and provides evidence of the mixing among perturbations. In section 4 we show the results of the spectral analysis methods applied to the proposed dynamical indicators. Section 5 is devoted to discussing and analyzing the results reported in the previous sections. In the appendix we report some preliminary results for the temporal correlations of the phase-space perturbations. We present our conclusions in section 6.

2. The model and simulation details

2.1. Phase-space dynamics

The LJ potential $U_{\mathrm{LJ}}(r)$ between particles i and j is given by

$$U_{\mathrm{LJ}}(r) = 4\epsilon\left[\left(\frac{\sigma}{r}\right)^{12} - \left(\frac{\sigma}{r}\right)^{6}\right], \tag{1}$$

where $r \equiv r_{ij}$ is the distance between particles i and j; here σ and ϵ are the LJ atom diameter and the strength of the interparticle interaction, respectively. The actual interaction potential employed in our simulations is the spherically truncated and shifted (STS) potential, which can be written as

$$U(r) = \begin{cases} U_{\mathrm{LJ}}(r) - U_{\mathrm{LJ}}(r_c) & r \leqslant r_c \\ 0 & r > r_c, \end{cases} \tag{2}$$

where $r_c = 2.5\sigma$ is the cut-off radius at which the potential is truncated in order to save computer time. It is important to note that the force derived from the above potential, as well

as its derivative, is not continuous at the truncation point r_c. Therefore the following potential, first proposed in [27], can be employed:

$$U(r) = \begin{cases} 4\epsilon\left[\left(\frac{\sigma}{r}\right)^{12} - \left(\frac{\sigma}{r}\right)^{6}\right] + c_2\left(\frac{r}{r_c}\right)^2 + U_c & r \leqslant r_c \\ 0 & r > r_c, \end{cases} \tag{3}$$

with $c_2 = 4\epsilon[6(\sigma/r_c)^{12} - 3(\sigma/r_c)^6]$ and $U_c = 4\epsilon[-7(\sigma/r_c)^{12} + 4(\sigma/r_c)^6]$. This potential has a continuous derivative at the truncation point r_c. Nevertheless, for the 1D LJ model it has been shown, by adopting the above expression for the potential, that the qualitative behavior of the LMs is not greatly affected by the discontinuity of the STS potential at r_c [20]. In the next section it will be shown explicitly that this same phenomenology holds for our 3D LJ fluid. The complete Hamiltonian of our system is then

$$H = \sum_{i=1}^{N} \frac{p_i^2}{2m_i} + \sum_{i<j} U(r_{ij}), \tag{4}$$

with $\{\mathbf{p}_i\}$ being the momenta of the atoms and $\{m_i\}$ their corresponding masses. In all our simulations we took the masses of the atoms equal to unity, i.e. $m_i = m = 1\ \forall\ i$, with $\sigma = 1$, and $\epsilon = 1$ as well. The Hamiltonian is then written in terms of the reduced variables $r^* = r/\sigma$, $p_i^* = p_i/(m\epsilon)^{1/2}$ and $m_i^* = m_i/m$.

The initial configuration for all simulations was set up from a fcc lattice on a square cell of sides $L^* = L_x^* = L_y^* = L_z^*$. The initial momenta were drawn from a Maxwell–Boltzmann distribution. Then the $6N$ equations of motion were numerically integrated by means of the Verlet leap-frog algorithm with periodic boundary conditions and the minimum image convention applied in all directions. A time-step of $\Delta t^* = \Delta t(\epsilon/m)^{1/2}/\sigma = 0.001$ was used in all simulations, with an equilibration period of 100 000 steps at constant temperature obtained by a uniform rescaling of the velocities at each time-step. After the equilibration period the system was allowed to evolve at constant total energy for a period of 10^6 time-steps. The relative energy drift for this number of time-steps is 10^{-4}–10^{-5}, which is an acceptable compromise between accuracy and speed, since there is no systematic drift, and thus the energy fluctuations are stable for the chosen time-step. All the reported results were obtained for systems of $N = 108$ at a supercritical reduced temperature of $T^* = k_B T/\epsilon = 1.5$, where k_B is the Boltzmann constant. The reduced densities $\rho^* = \rho\sigma^3$ were taken within the range $\rho^* \in [0.01, 0.5]$. The critical temperature and density for the LJ fluid with STS potential are $T_c^* = 1.085$ and $\rho_c^* = 0.317$ [28]; thus the employed values for these variables ensure that the system state is far away from the two-phase region in the ρ^* versus T^* phase diagram, being a homogeneous fluid. Finally, since in the rest of the work reduced variables will be exclusively employed, from now on we will drop the asterisk from all symbols without the risk of confusion.

2.2. *Tangent-space dynamics*

The phase-space trajectory is represented by the variable $\mathbf{\Gamma}(t) \equiv (\mathbf{\Gamma}_1(t), \mathbf{\Gamma}_2(t), \ldots, \mathbf{\Gamma}_N(t))$, where $\mathbf{\Gamma}_i(t) \equiv (\mathbf{r}_i(t), \mathbf{p}_i(t))$. To study the local dynamical stability of our system we introduce the *Lyapunov vector* (LV) as $\delta\mathbf{\Gamma}^{(\alpha)}(t) \equiv \left(\delta\mathbf{\Gamma}_1^{(\alpha)}(t), \delta\mathbf{\Gamma}_2^{(\alpha)}(t), \ldots, \delta\mathbf{\Gamma}_N^{(\alpha)}(t)\right)$, where $\alpha = 1, \ldots, 6N$ and $\delta\mathbf{\Gamma}_i^{(\alpha)}(t) \equiv \left(\delta\mathbf{r}_i^{\alpha}(t), \delta\mathbf{p}_i^{\alpha}(t)\right)$ representing the ith particle contribution to the infinitesimal perturbations of the trajectory $\mathbf{\Gamma}(t)$ along all possible directions (position and momentum axes) of the phase space, thus defining the so-called *tangent space*.

According to Oseledec's multiplicative ergodic theorem [29] the remote past limit symmetric operator $\Phi_b(t) = \lim_{t_0\to-\infty}[\mathcal{M}(t,t_0)\cdot\mathcal{M}^T(t,t_0)]^{1/[2(t-t_0)]}$ exists for almost every initial condition $\mathbf{\Gamma}(t_0)$, where $\mathcal{M}(t,t_0)$ is the fundamental matrix governing the time evolution of the perturbations $\delta\mathbf{\Gamma}(t)$ in tangent space as $\delta\mathbf{\Gamma}(t) = \mathcal{M}(t,t_0)\cdot\delta\mathbf{\Gamma}(t_0)$ [10]. The set of instantaneous LEs is defined as $\lambda^{(\alpha)}(t) = \ln\Lambda^{(\alpha)}$, where $\Lambda^{(\alpha)}$ are the eigenvalues of $\Phi_b(t)$. The herein employed standard procedure for computing the LEs consists in periodically reorthonormalizing a set of offset vectors that are time-evolved by means of the matrix $\mathcal{M}(t,t_0)$ [30, 31]. The time-averaged values of the logarithms of the renormalization factors, i.e. $\langle\ln\Lambda^{(\alpha)}\rangle_t$ are the LEs $\{\lambda^{(\alpha)}\}$ and the set of offset vectors right after the reorthonormalization are the eigenvectors of $\Phi_b(t)$, which are called *backward* LVs. The equivalence of the LEs computed by means of these two methods can be proved rigorously [32], but the relation between the Oseledec eigenvectors and the LVs obtained via the standard method is more subtle. It is known that the backward LVs converge at an exponential rate to the Oseledec eigenvectors for the inverse-time dynamics of the original system [33, 34]. The latter are obtained as the eigenvectors of the far future limit operator $\Phi_f(t) = \lim_{t_0\to\infty}[\mathcal{M}^T(t_0,t)\cdot\mathcal{M}(t_0,t)]^{1/[2(t_0-t)]}$ and are called *forward* LVs. It is to be noted that recently it has been possible to obtain from the intersection of the embedded subspaces spanned by the eigenvectors of $\Phi_b(t)$ (backward LVs) and $\Phi_f(t)$ (forward LVs) the so-called *characteristic* LVs, which are independent of the norm and do not form an orthogonal basis [35]. A somewhat similar algorithm has also been proposed in [36]. The aforementioned schemes are based on ideas already discussed long ago [37], but have only been recently proposed because their implementation is by no means a simple task from a computational point of view, which is why they only have been tested in simple 1D systems. Thus it is not at all clear that their implementation could be feasible in the near future for the case of our system. Furthermore, since the purpose of the present work is to investigate the possible existence of LMs in a 3D LJ fluid, it is important to recall that the discovery of LMs in all studied systems so far has been made employing the backward LVs. So it seems that the use of the CLVs is not essential for the detection of LMs. Finally, meaningful results are still obtained by means of the backward LVs obtained from the standard procedure, such as in the recent characterization of LMs in a diatomic system [38] and the discovery of LMs in the XY rotator model [39]; in both studies the backward LVs were employed. Therefore, from now on we will refer to the numerically computed vectors (backward LVs) as the LVs without confusion.

In the Hamiltonian case (which we treat here), and also in some special homogeneous non-equilibrium situations [40], the LEs and the corresponding LVs have a symmetry property which makes it unnecessary to calculate the whole spectrum. In these cases the LS thus computed is symmetrical around zero, which means that each LE has a partner that is exactly its negative. This is the so-called *conjugate-pairing rule* [41]. Therefore, only $3N$ linearized equations for the LVs were simultaneously integrated, along with the $6N$ nonlinear equations for the reference trajectory $\mathbf{\Gamma}(t)$. The initial LVs $\delta\mathbf{\Gamma}^{(\alpha)}(t_0)$ in all our simulations consisted of a set of $3N$ orthogonal vectors with randomly selected components.

3. Lyapunov spectrum

As mentioned in the previous section, both the force derived from the STS potential and its derivative are not continuous at r_c. In order to assess the relevance of this particular feature in the computation of the properties in the tangent space we perform additional simulations employing the potential given by equation (3). In figure 1 we present the LS computed from this last potential, as well as that computed by means of the STS potential, for $T = 1.5$, $\rho = 0.1$

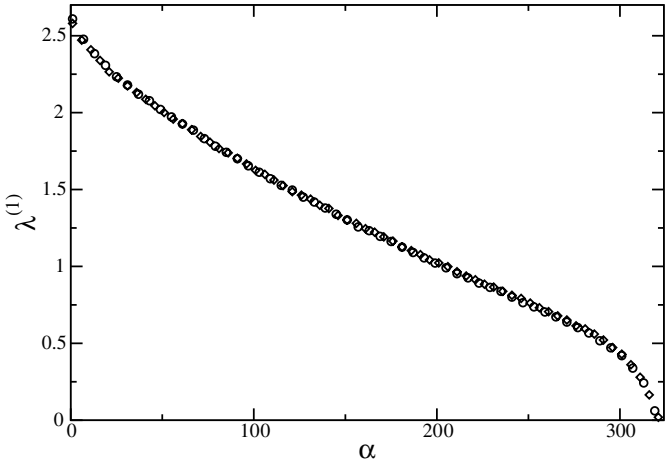

Figure 1. LS $\{\lambda^{(\alpha)}\}$ as a function of the Lyapunov index α computed for a system with the STS potential (circles) and the potential defined by equation (3) (diamonds). The thermodynamic state in both cases is defined by $\rho = 0.1$ and $T = 1.5$, with $N = 108$.

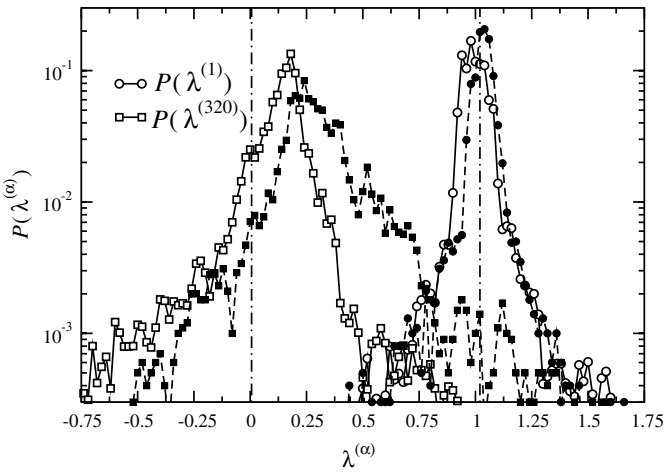

Figure 2. Probability density function of the instantaneous LEs $\lambda^{(1)} = 1.014$ (circles) and $\lambda^{(320)} = 0.011$ (squares) for $\rho = 0.01$. Filled symbols correspond to the results obtained with the potential given by equation (3). Average taken over 2×10^6 integration time-steps. Same N and T values as in figure 1. Vertical dot-dashed lines indicate the values for $\lambda^{(1)}$ and $\lambda^{(320)}$.

and $N = 108$. As can be readily appreciated there are no significant differences, a result which supports the use of the simpler STS potential. The most relevant feature of this figure is that, as in the case of the 1D LJ gas, in the smallest positive LE region there is no evidence of the stepwise structure that signals the appearance of the LMs in the case of hard-core systems. Thus, it is plausible that the same mechanism that accounts for the absence of the stepwise structure in the LS of the 1D LJ gas is also at work in the present model.

In figure 2, we present the probability density function for the instantaneous LEs $\lambda^{(1)}$ and $\lambda^{(320)}$ for $N = 108$ and $\rho = 0.01$. It can be observed that the fluctuations around their

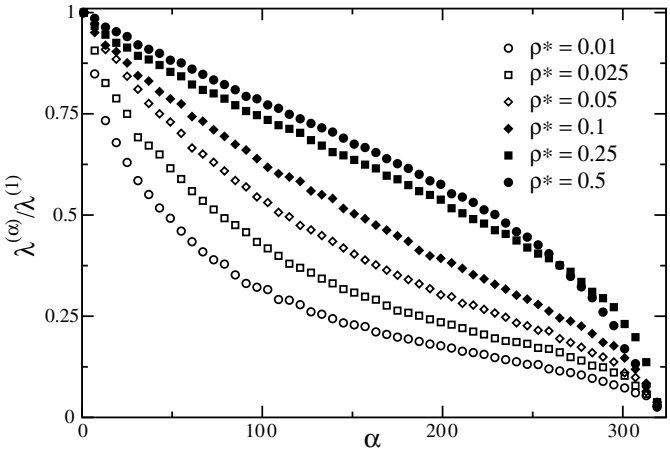

Figure 3. Normalized LS $\{\lambda^{(\alpha)}/\lambda^{(1)}\}$ as a function of the Lyapunov index α for all employed values of the reduced density ρ and a reduced temperature of $T = 1.5$, with $N = 108$.

Table 1. Length L of the cubic simulation cell along with the values of the LLE for each reduced density value.

ρ	L	λ_1
0.01	22.104	1.014
0.025	16.287	1.531
0.05	12.927	2.033
0.1	10.260	2.606
0.25	7.560	3.496
0.5	6.000	4.349

mean values increase as the Lyapunov index α increases, i.e. when going from a high to a low value of the LE. It is to be observed that the fluctuations in the $\lambda^{(320)}$ value are so great that the tails in the probability density function overlap with those corresponding to $\lambda^{(1)}$. These large fluctuations are certainly a reason why no stepwise structure can be found in the low-α region of the LS. Other dynamical indicators that we will present later on are also affected by this behavior of the LS at large α values. In the same figure results for the potential given by equation (3) are also presented; these are quite similar to those obtained with the STS potential. Thus it is confirmed that the aforementioned fluctuations are not a result of the discontinuity of the STS potential at r_c. Therefore this potential will be used in the rest of this work. Other dynamical indicators that we will present later on are also affected by this behavior of the LS at large α values.

In figure 3 we show the normalized LS for $N = 108$ and $T = 1.5$ computed for the employed range of reduced densities. The values of the scalar length of an edge of the cubic simulation cell, as well as the values of the LLE corresponding to each value of the reduced density, are reported in table 1. As can be readily appreciated in figure 3, the LS $\{\lambda^{(\alpha)}\}$ corresponding to the lowest density $\rho = 0.01$ can be separated into two regions. In both of them the LS is a decreasing function of the Lyapunov index α, but in the former the decrease is more pronounced than in the latter. This bending of the LS has been observed in a quasi-1D

hard-disk gas [42] as well as in the 1D LJ gas [20], and has been related to the separation of two timescales. To properly explain this point it is important to remember that each LE indicates a timescale given by its inverse, so the LS can be considered as a spectrum of timescales. The smallest positive LE region of the spectrum is dominated by macroscopic time and length scale behavior. On the other hand, the opposite region of the LS is dominated by short timescale behavior, such as local collision events. As the density increases, the collisions increase both in frequency and in the number of particles involved; the correlation among them increases, and becomes increasingly difficult to distinguish them individually. Thus it is no longer possible to make a separation of timescales, and so the LS does not present the aforementioned bending for $\rho \geqslant 0.1$. Although this explanation is plausible for the LS of our 3D LJ fluid, we also point out that the bending depicted in figure 3 for $\rho = 0.01$ (the lowest reduced density value employed) is less pronounced than the corresponding lowest density instance of the LS of the 1D LJ gas [20]. We interpret this fact as a signature that, even for the lowest density case, the effect of the dimensionality in the microscopic events is to enhance the correlation among them, and thus reduce the separation of timescales that is more evident in the 1D case. This explanation will be further supported in the next sections.

4. Spatial structure of tangent-space perturbations

4.1. Spatial Lyapunov vector density

As discussed in section 3, the strong fluctuations of the smaller LEs make the perturbations in tangent space extremely unstable, rendering any coherent structure that may exist in configuration space difficult to detect. To investigate the possibility that these structures (LMs) exist in the case of the 3D STS LJ potential we have to establish a measure of the contribution of a given LV $\delta\mathbf{\Gamma}^{(\alpha)}(t)$ at each point $\mathbf{r}$ of the configuration space, regardless of which particle makes the contribution to the magnitude of the chosen LV. We have to remember that the ith particle contribution to the infinitesimal perturbation $\delta\mathbf{\Gamma}^{(\alpha)}(t)$ consists of spatial and momentum components. Since the LMs can be in general considered as Goldstone modes resulting from translational invariance in coordinate space [18], we will consider only the spatial part of the full perturbation component $\delta\mathbf{\Gamma}_i^{(\alpha)}(t)$. Thus, in analogy with the definition of microscopic density fluctuations [43], we define the *spatial LV density* as

$$\mathbf{u}^{(\alpha)}(\mathbf{r}, t) = \sum_{i=1}^{N} \delta\mathbf{r}_i^{(\alpha)} \delta(\mathbf{r} - \mathbf{r}_i), \tag{5}$$

which was first introduced in [44] and is the function to be studied afterward. In figure 4, we present a snapshot of a single component $u_z^{(\alpha)}(z, t) = \sum_{i=1}^{N} \delta z_i^{(\alpha)} \delta(\mathbf{r} - \mathbf{r}_i)$ of the aforementioned spatial density along the z-axis of our system. Since the latter is isotropic, the results are completely analogous to those corresponding to the $u_x^{(\alpha)}$ and $u_y^{(\alpha)}$ components projected along their respective coordinate axes. We can readily appreciate that the spatial density corresponding to the LLE is more localized than that corresponding to the LE with $\alpha = 320$, which is the lowest index value corresponding to a LV not related to the space and time translational invariance symmetries of the system and the associated conserved quantities, the total energy and the total momentum [17]. A point to be noted is that the localization of the LLE is not so clearly defined and strong as in the 1D LJ system [20] or in hard-disk systems [42]. This is another indication that the dimensionality of the system has indeed a strong influence on the tangent-space dynamics.

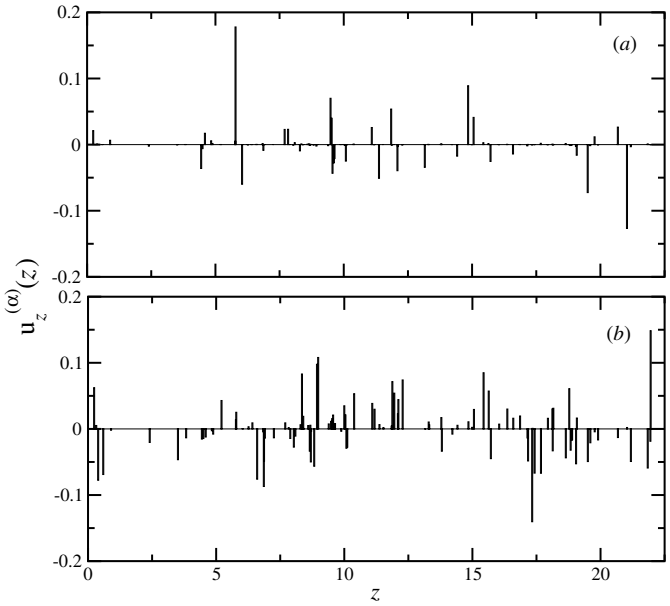

Figure 4. Snapshot of the spatial LV density component $u_z^{(\alpha)}(z, t)$ along the z-axis of the simulation box for a LJ fluid of $N = 108$ atoms at a reduced density of $\rho = 0.01$ corresponding to the LVs: (*a*) $\alpha = 1$ and (*b*) $\alpha = 320$.

Next, we proceed to consider the spatial Fourier transform of $\mathbf{u}^{(\alpha)}(\mathbf{r}, t)$, which can be written as

$$\begin{aligned}\widetilde{\mathbf{u}}^{(\alpha)}(\mathbf{k}, t) &= \int \mathbf{u}^{(\alpha)}(\mathbf{r}, t) \exp(-\mathrm{i}\mathbf{k}\cdot\mathbf{r})\, \mathrm{d}\mathbf{r} \\ &= \sum_{i=1}^{N} \delta\mathbf{r}_i^{(\alpha)} \exp[-\mathrm{i}\mathbf{k}\cdot\mathbf{r}_i(t)].\end{aligned}$$

To proceed further we invoke the *static LV density correlation function* of [44], defined as

$$\mathcal{C}^{(\alpha)}(\mathbf{k}, t) \equiv \widetilde{\mathbf{u}}^{(\alpha)}(\mathbf{k}, t)\widetilde{\mathbf{u}}^{(\alpha)}(-\mathbf{k}, t), \tag{6}$$

which in the case of our 3D system is a second-rank tensor. For our isotropic fluid the Cartesian components $C_{\mu\nu}^{(\alpha)}(\mathbf{k}, t)$ of $\mathcal{C}^{(\alpha)}(\mathbf{k}, t)$ can be written in terms of longitudinal $C_L^{(\alpha)}$ and transverse $C_T^{(\alpha)}$ static correlation functions as

$$C_{\mu\nu}^{(\alpha)}(\mathbf{k}, t) = \hat{k}_\mu \hat{k}_\nu C_L^{(\alpha)}(\mathbf{k}, t) + (\delta_{\mu\nu} - \hat{k}_\mu \hat{k}_\nu) C_T^{(\alpha)}(\mathbf{k}, t), \tag{7}$$

with $\hat{k}_\mu = (\mathbf{k}/k)_\mu$. From this last expression it is immediate to obtain the explicit form of the longitudinal and transverse static correlation functions as

$$\begin{aligned}C_L^{(\alpha)}(\mathbf{k}, t) &= C_{\mu\nu}^{(\alpha)}(\mathbf{k}, t)\hat{k}_\nu \hat{k}_\mu \\ C_T^{(\alpha)}(\mathbf{k}, t) &= \tfrac{1}{2}\left(C_{\nu\nu}^{(\alpha)}(\mathbf{k}, t) - C_{\mu\nu}^{(\alpha)}(\mathbf{k}, t)\hat{k}_\nu \hat{k}_\mu\right).\end{aligned}$$

To simplify the analysis we will consider a coordinate system such that the wave vector $\mathbf{k}$ is parallel to the z-axis. Then

$$\widetilde{\mathbf{u}}^{(\alpha)}(\mathbf{k}, t) = \sum_{i=1}^{N} \delta\mathbf{r}_i^{(\alpha)} \exp[-\mathrm{i}k_z z_i(t)]. \tag{8}$$

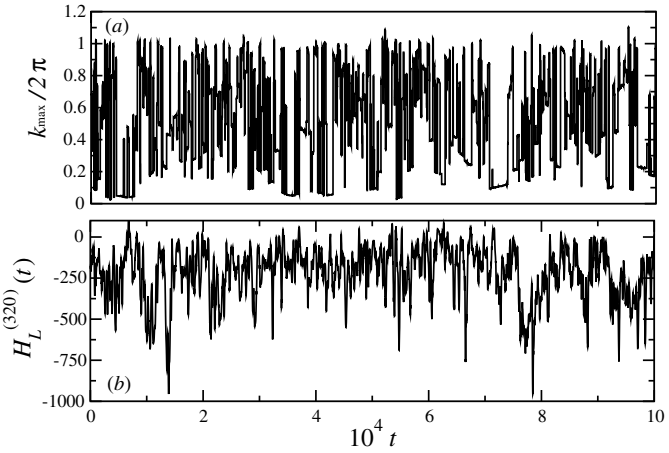

Figure 5. (*a*) Time evolution of the peak wave-number $k_{\max}$ and (*b*) spectral entropy $H_L^{(\alpha)}(t)$ for a Lyapunov index value of $\alpha = 320$, for $N = 108$, $\rho = 0.01$ and $T = 1.5$. The behavior of these quantities corresponding to the transverse correlation function $C_T^{(\alpha)}(k, t)$ (not shown) is almost the same as that depicted in the above figure.

For homogeneous systems with translational invariance the Fourier transformed components of a quantity such as the spatial LV density $\{\widetilde{u}_\nu^{(\alpha)}\}$, where $\nu = x, y, z$, are uncorrelated [45]. Thus, our simplification in no way destroys essential information. The spatial Fourier spectrum $P_{\nu\nu}^{(\alpha)}(k_z, t) \equiv \left|\widetilde{u}_\nu^{(\alpha)}(k_z, t)\right|^2$ corresponding to each component of the spatial density of $\delta\mathbf{r}_i^{(\alpha)}$ can be readily computed by an algorithm for unequally spaced data points [46], which has been previously applied to the 1D LJ [20] and the 2D WCA systems [21]. Furthermore, we observe that the diagonal components of the static LV density correlation function correspond to the spatial Fourier spectrum, i.e. $C_{\nu\nu}^{(\alpha)}(k_z, t) \equiv P_{\nu\nu}^{(\alpha)}(k_z, t)$. Thus the static longitudinal and transverse correlation functions can be obtained from the aforementioned power spectra as

$$C_L^{(\alpha)}(k_z, t) = P_{zz}^{(\alpha)}(k_z, t)$$
$$C_T^{(\alpha)}(k_z, t) = \tfrac{1}{2}\left(P_{xx}^{(\alpha)}(k_z, t) + P_{yy}^{(\alpha)}(k_z, t)\right).$$

Finally, since averaging over several spatially equivalent directions will improve the statistics, we take successively the **k** vector along the remaining coordinate axes x and y to obtain two more sets of longitudinal and transverse correlation functions and then average over all sets. The result is longitudinal $C_L^{(\alpha)}(k, t)$ and transverse $C_T^{(\alpha)}(k, t)$ correlation functions independent of the employed coordinate system.

At variance with the hard-core systems in which the patterns resembling transverse modes do not survive time averaging [19], the Fourier spectral techniques so far presented have been quite successful in the case of the 1D LJ system, and so there is a reasonable possibility of success in the case of our 3D LJ fluid.

4.2. Time instability of instantaneous quantities

Due to their mutual interaction, the LMs in all soft potential systems are only of finite life-time. To investigate their time stability we present in figure 5 the time evolution of two quantities associated with the longitudinal static correlation function $C_L^{(\alpha)}(k, t)$ for the LV $\alpha = 320$: the peak wave number $k_{\max}$, which indicates the position of the highest peak in the spatial Fourier

spectrum $P_{zz}^{(\alpha)}(k,t)$, and the *spectral entropy* $H_L^{(\alpha)}(t)$ [47], which measures the k distribution properties of the aforementioned spectrum. This last quantity was first employed in [20] in the study of the 1D LJ gas and is defined as

$$H_L^{(\alpha)}(t) = -\sum_k C_L^{(\alpha)}(k,t) \ln C_L^{(\alpha)}(k,t). \tag{9}$$

For the 1D LJ system these quantities show an intermittent behavior, i.e. large intervals of nearly constant low values (*off state*) are interrupted by short periods of bursts (*on state*) where they experience large values [20]. As can be appreciated in figure 5(*a*) for the time evolution of the peak wave number $k_{\max}$, this behavior is somewhat different in our case; although there is an alternation between the on- and off-states, the mixing among them is so great that there are no long-lived time intervals for either state, in sharp contrast to the 1D case. The instant value of the spectral entropy, presented in figure 5(*b*), has a similar behavior as that of $k_{\max}$ in the sense that it is not easy to identify a correspondence between its temporal evolution and that of the on- and off-states. A virtually identical behavior is obtained for $k_{\max}$ and $H_T^{(\alpha)}(t)$, but now defined in terms of $C_T^{(\alpha)}(k,t)$ (not shown), and for all values of the reduced density. This intermittency in the time evolution of the spatial Fourier spectrum of LVs is a typical feature of soft-potential systems. However, this behavior is greatly increased in comparison to the 1D case. There are two possible causes for this difference with the 1D results: first, the reduced temperature at which we are working is much higher (an order of magnitude) than that employed in [20]; second, the dimensionality of our system is also higher, thus the mixing is easier by this enlargement in the phase space, as already explained. Now, in order to average out temporal fluctuations, and thus extract useful information about the collective modes, from now on we will study the properties of the average spectra $\left\langle C_L^{(\alpha)}(k,t)\right\rangle_t$ and $\left\langle C_T^{(\alpha)}(k,t)\right\rangle_t$, where $\langle\cdots\rangle_t$ means temporal average. Further insight into the temporal dynamics of the LMs can be obtained by studying the dynamic LV density correlation function first introduced in [44] for the 1D LJ gas. In the appendix some preliminary results of the aforementioned dynamical correlation function applied to our 3D LJ fluid will be presented.

4.3. Time-averaged power spectrum

Figures 6(*a*) and (*b*) display, for $\rho = 0.01$, $\left\langle C_L^{(\alpha)}(k,t)\right\rangle_t$ and $\left\langle C_T^{(\alpha)}(k,t)\right\rangle_t$, respectively. In both cases we can readily appreciate that the contribution of the high-wave-number components is not small. The instantaneous power spectra are not dominated by a single peak; rather, several small peaks, which are related to intermediate length scales, are present, which in turn make significant contributions to the overall shape of the time-averaged correlation functions for large k values. This feature can be explained by the less pronounced timescale separation than in the 1D case, as mentioned in section 3 in relation to the LS. Nevertheless, the highest value of the time-averaged correlation functions is always dominated by certain low-wave-number components; for the longitudinal correlation function we observe that the sharp-valued peak in the spectrum corresponds to diminishing $k_{\max}$ values as the Lyapunov index $\alpha \to 3N$, i.e. as we go from the region of high LEs to the region of low LEs. At this point it is important to note that this correspondence is not monotonic, since the $k_{\max}$ value of the highest peak is attained at $\alpha = 200$, and the height of the corresponding peak slightly diminishes, although remains well defined, for higher α values. For the transverse correlation function depicted in figure 6(*b*) the results are similar, except for a very important feature: the highest value of the spectra is again attained at $\alpha = 200$, a value far away of the region corresponding to the lowest LEs, but then vanishes as $\alpha \to 3N$. This feature is not consistent with the existence of well-defined transverse LMs, since it would be expected that the highest peak in the transverse

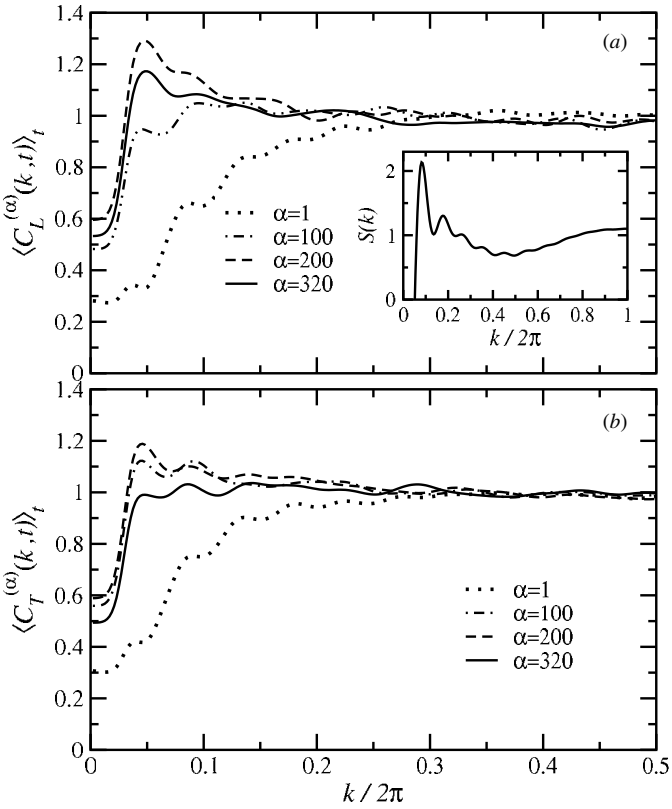

Figure 6. (*a*) The time-averaged longitudinal correlation function $\langle C_L^{(\alpha)}(k,t)\rangle_t$ and (*b*) the time-averaged transverse correlation function $\langle C_T^{(\alpha)}(k,t)\rangle_t$ for various values of the Lyapunov index α, with parameters $N = 108$, $T = 1.5$ and $\rho = 0.01$. In the inset the static structure factor $S(k)$ of the system is plotted.

correlation function should correspond to small values of $k_{\max}$ in the $\alpha \approx 3N$ regime. In the inset the static structure factor $S(k)$ [43] for the corresponding thermodynamic state is plotted. The highest peak of this function is located at $k/2\pi \approx 0.08$. Now, the position of the peak in $\left\langle C_L^{(\alpha)}(k,t)\right\rangle_t$ is located at $k_{\max} \approx 0.04$. This value suggests that there is no obvious direct connection between the short-range order of the atoms and the lowest wave vector peak of the longitudinal LV correlation function.

The longitudinal and transverse correlation functions corresponding to the reduced density $\rho = 0.5$ are presented in figures 7(*a*) and (*b*), respectively. A difference with respect to the low density results is that the highest peak in each power spectrum is broader than in the corresponding low-density case. This can be interpreted as an indication that the influence of higher wave numbers is stronger than in the low-density case. We further observe that the highest peak is located at a higher wave number value than the corresponding peaks in figures 6(*a*) and (*b*). Now, although at this density there is a higher degree of spatial order in the atoms of the system, the lowest wave vector peak of $S(k)$, which is plotted in the inset, has no relation whatsoever with the $k_{\max}$ value of the time-averaged transverse LV correlation function. Next we note that the highest peak of the transverse correlation function is reached at a value of the Lyapunov index of $\alpha = 200$, with a monotonic decrease for higher α values. This same result was obtained for the transverse correlation function in the low-density regime,

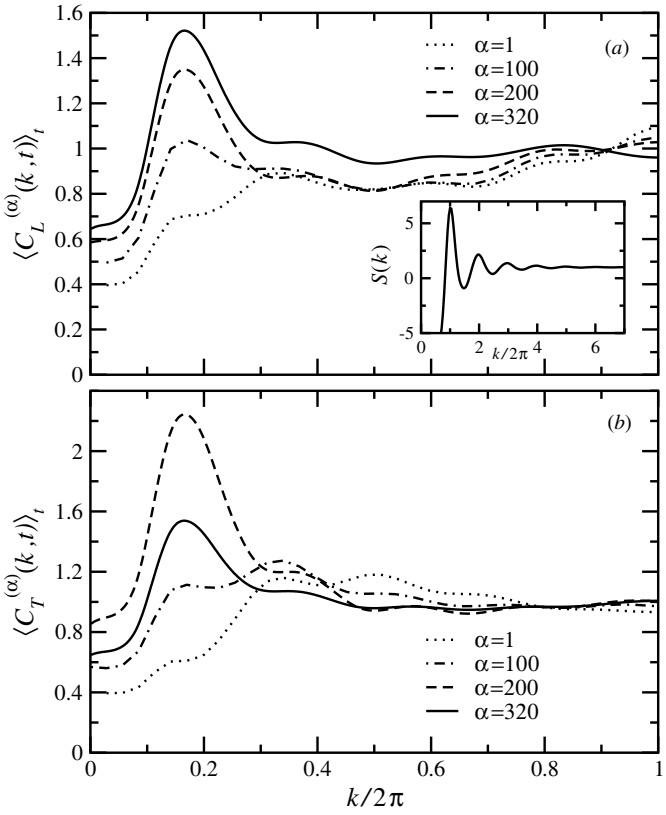

Figure 7. (*a*) Time-averaged longitudinal and (*b*) transverse correlation functions for the same parameters as in figure 6, but with a reduced density of $\rho = 0.5$.

although in this case the peak remains well defined, in contrast to the result displayed in figure 6(*b*), which is almost a flat spectrum.

So far our results are consistent with the existence of longitudinal LMs. To quantify the properties of these modes in figure 8(*a*) we plot $k_{\max}$ versus the Lyapunov index α. It is clear from this figure that, as $\alpha \to 3N$, $k_{\max}$ diminishes. A feature that stands out is that, despite the time averaging over a large number of data points (10^6 time steps), the obtained values remain somewhat noisy. Nevertheless it is clear from the figure that the decrease in the $k_{\max}$ value as α increases is approximately monotonic, in clear contrast to the 1D case [20] in which a sudden change of $k_{\max}$ from a finite value to zero was interpreted as a signature of the separation of timescales mentioned in section 3. Next, in figure 8(*b*) the height $\left\langle C_L^{(\alpha)}(k_{\max}, t)\right\rangle_t$ of the highest peak in the time-averaged longitudinal correlation function is also plotted as a function of the Lyapunov index α. On average we can observe a monotonic increase of the peak value as the Lyapunov index α goes from small to large values, although a small decrease can be noticed in the $\alpha \approx 3N$ region. Finally, from the definition given in equation (9), it is immediate to obtain the average spectral entropy $\langle H_L\rangle_t$ which is presented, again as a function of α, in figure 8(*c*). Its value decreases as the Lyapunov index increases. This in turn means that LVs corresponding to smaller positive LEs are more localized in Fourier space, i.e. they have more wave-like character than those corresponding to larger LEs. However, the decrease in the value of $\langle H_L\rangle_t$ as the Lyapunov index increases is not monotonic. We note that already

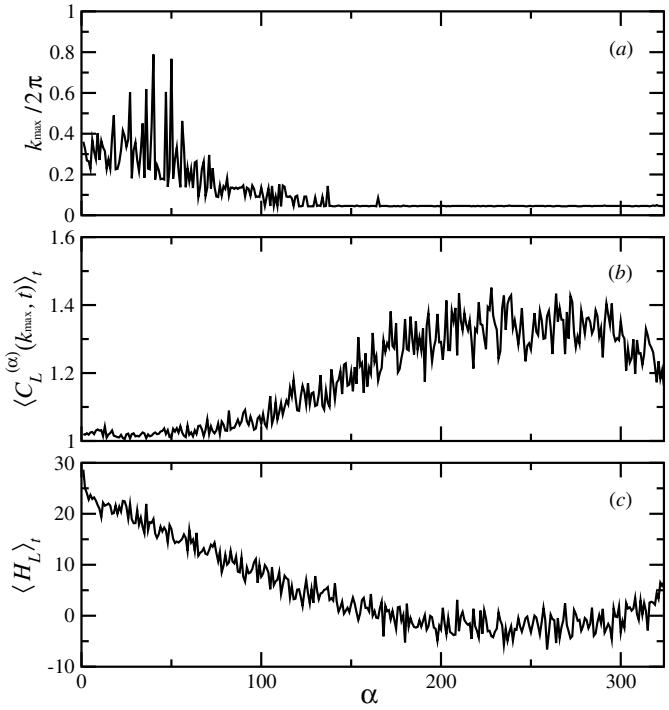

Figure 8. (*a*) Wave number $k_{\max}$ of the highest peak in the time-averaged longitudinal correlation function $\langle C_L^{(\alpha)}(k,t)\rangle_t$ for each α value. (*b*) The height $\langle C_L^{(\alpha)}(k_{\max},t)\rangle_t$ of the highest peak in the time-averaged correlation function. (*c*) Average spectral entropy $\langle H_L\rangle_t$. The parameters are $\rho = 0.01$, $N = 108$ and $T = 1.5$.

for $\alpha = 200$ the average spectral entropy has reached its minimum value, but presents a slight increase as $\alpha \to 3N$, which certainly accounts for the decrease in the height of the peak in the average spectra of figure 6(*a*). Our tentative conclusion at this point is that the longitudinal LMs are more vaguely defined than in the 1D case for this density value.

The results corresponding to the transverse correlation function $\left\langle C_T^{(\alpha)}(k,t)\right\rangle_t$ are presented in figure 9. We observe that the α range for which $k_{\max}$ has a small value is broader compared to the results in figure 8(*a*). However, $k_{\max}$ has a slight increase in value as $\alpha \approx 3N$, a result which is not consistent with the existence of a transverse Lyapunov mode for this α range. This conjecture is supported by the behavior of $\left\langle C_T^{(\alpha)}(k_{\max},t)\right\rangle_t$ displayed in figure 9(*b*). This last quantity has its maximum at $\alpha \approx 200$, with a corresponding minimum of $\langle H_T\rangle_t$ at the same α value, as seen in figure 9(*c*). This feature of the spectral entropy is inconsistent with localization in Fourier space; that is, the wave-like character of the LVs is largely diminished in the low-α region. Taken together these results make it difficult for us to unambiguously ascertain the existence of transverse LMs in the 3D LJ system.

For the case of high reduced density $\rho = 0.5$ figure 10(*a*) presents the results for $k_{\max}$ versus the Lyapunov index α corresponding to the longitudinal correlation function $\left\langle C_L^{(\alpha)}(k,t)\right\rangle_t$. The behavior displayed is very different to that shown in figure 8(*a*). We first note that the fluctuations of all quantities are much smaller than those corresponding to the low-density value. In the present case the value of $k_{\max}$ stays close to 1 for $\alpha \lesssim 100$. Then, as α further increases and after a small transient interval, $k_{\max}$ drops rather sharply to a

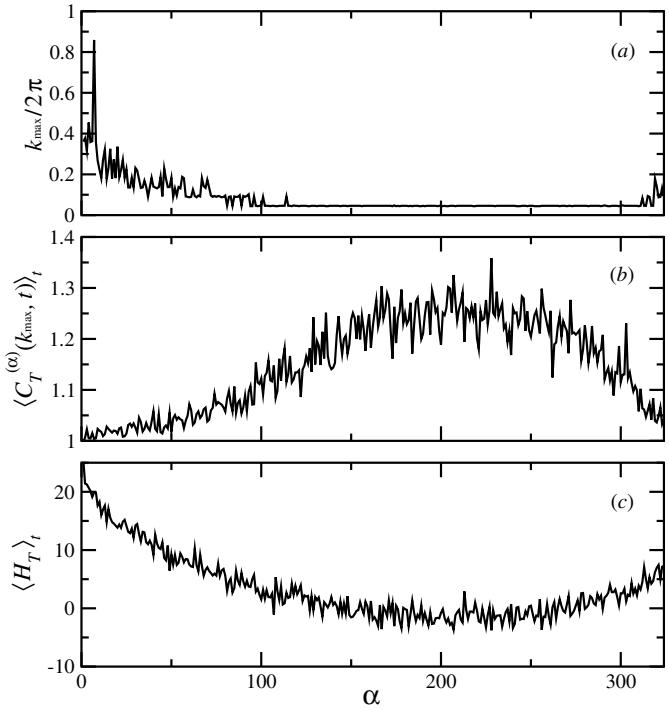

Figure 9. Same variables as in figure 8, but corresponding to the time-averaged transversal correlation function $\langle C_T^{(\alpha)}(k,t)\rangle_t$. Same values of N, ρ and T as in figure 8.

value slightly lower than 0.2, which is consistent with that obtained from figure 7(*a*). Next, in figure 10(*b*) we observe that the value of $\left\langle C_L^{(\alpha)}(k_{\max},t)\right\rangle_t$ decreases smoothly from its maximum at $\alpha \approx 3N$ down to its minimum at $\alpha \approx 100$. Finally, in figure 10(*c*) we observe that, at variance with the low-density result, the value of the average spectral entropy $\langle H_L\rangle_t$ decreases monotonically in the whole range of α values, with a minimum for $\alpha \approx 3N$ where the LEs are the smallest possible ones. From the definition of the spectral entropy we conclude that the corresponding spectra for these LVs are most significantly dominated by a few k values. Thus the LMs are more sharply defined than in the low-density case: a very intriguing state of affairs, since no relation was found between the spatial order of the atoms as described by $S(k)$ and the highest peak in the LV power spectrum at any density value.

The results for the transverse correlation function $\left\langle C_T^{(\alpha)}(k,t)\right\rangle_t$ for the highest density studied are presented in figure 11, which display a much reduced fluctuation level, but have nevertheless a very similar behavior, compared to those in figure 9 corresponding to the low-density case. That is, the maximum value of $\left\langle C_T^{(\alpha)}(k_{\max},t)\right\rangle_t$, which is coincident with the minimum value of $\langle H_T\rangle_t$, is present in a range of α values that is far from the region in which $\alpha \approx 3N$, a result not entirely consistent with the existence of transverse LMs.

5. Discussion

The overall picture that emerges from our results so far indicates a tangent-space dynamics much more complicated than that of hard-core systems or the 1D LJ fluid. The strong

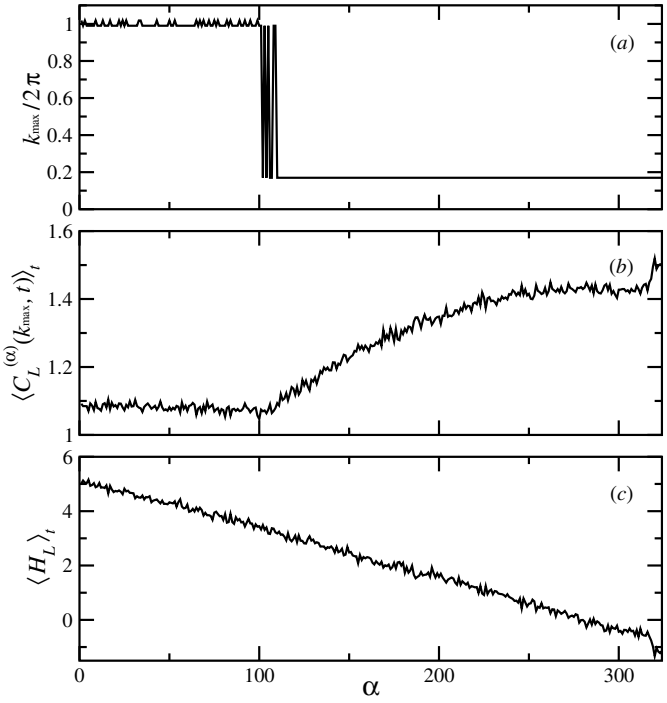

Figure 10. Same variables as in figure 8 for the time-averaged longitudinal correlation function $\langle C_L^{(\alpha)}(k,t)\rangle_t$ corresponding to the high-density value $\rho = 0.5$.

fluctuations in the LEs mentioned in section 3 produce a strong mixture among modes, so it is unreasonable to expect that results of the spectral analysis could convey information concerning pure modes. Indeed, the maximum wave number $k_{\max}$ for both the longitudinal and transverse correlation functions is highly unstable. In the time interval depicted in figure 5 for the longitudinal case the $k_{\max}$ value very rarely stays close to zero. Rather, it seems to wander randomly between zero and one. The instantaneous value of the spectral entropy, equation (9), also seems to have a seemingly random time evolution. Finally, there seems to be no correlation between the time evolution of $k_{\max}$ and $H_L^{(\alpha)}(t)$, which was discovered in the case of the 1D LJ system and which greatly contributed to a clear-cut definition of the so-called on- and off-states [20]. This is a first indication that the detection of LMs becomes more difficult than in the corresponding 1D case.

It turns out that the time-averaged longitudinal and transverse correlation functions are the relevant variables from which meaningful information about the LMs can be obtained. This fact can be understood in terms of the Zwanzig–Mori formalism, in which the Fourier components of the fluctuation of a conserved density vary slowly for a small wave number [45]; from these 'slow' variables a meaningful description is then extracted. For the tangent-space dynamics the time-averaged longitudinal and transverse correlation functions can be considered as the 'slow' variables. The results presented in figures 6 and 7 show that this is indeed the case; the spectra are dominated by low-wave-number values, i.e. $k_{\max} \approx 0.04$ for $\rho = 0.01$ and $k_{\max} \approx 0.16$ for $\rho = 0.5$, both for longitudinal and transverse correlation functions, with a corresponding broader peak in the latter case. In both cases $k_{\max} \approx 2\pi/L$, which is the smallest nonzero wave number allowed by the periodic boundary conditions used

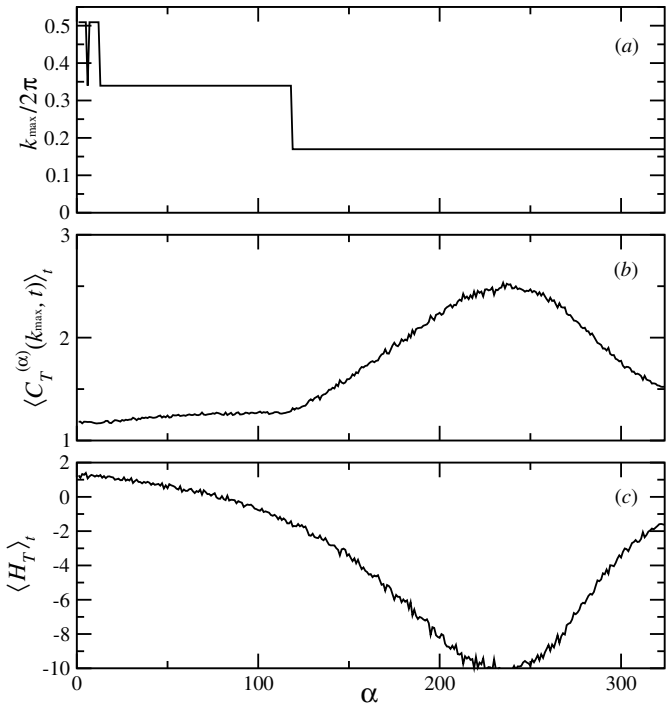

Figure 11. Same variables as in figure 8 for the time-averaged transverse correlation function $\langle C_T^{(\alpha)}(k,t)\rangle_t$ corresponding to the high-density value $\rho = 0.5$.

(smaller k values are due to the oversampling inherent to the method, see [46]). Another point to be noted is that, for our particular system, the longitudinal correlation function reaches its maximum value at $\alpha \approx 200$, and then its height diminishes slightly, but with the peak position k_{max} unchanged, as $\alpha \to 3N$. These results can be attributed to a complicate mixing of pure modes in the low-k regime, which produces the observed degeneracy of the k value with respect to the α index. Thus the obtained LMs lose their hydrodynamic character and no dispersion relation k_{max} versus $\lambda^{(\alpha)}$ as those observed in the 1D LJ fluid [20] and hard-core systems [48] could be detected. Our results even stand in contrast to those of 2D coupled map lattices, for which a dispersion relation $\lambda \sim k_{max}$ indeed exists [23], and even more sharply to those of the 2D LJ fluid, for which a corresponding dispersion relation has been claimed to hold, although for this last model the evidence seems so far to be inconclusive [44].

The most convincing evidence of the existence of longitudinal LMs for the low-density state comes from the results of figure 8. First we observe that the average spectral entropy attains its minimum at $\alpha \approx 200$, a result not entirely inconsistent with those of random matrix theory [14]. Next, as $\alpha \to 3N$, the value of this quantity remains close to this minimum. Taken together with the already obtained position of the highest peak in the power spectrum in the region $\alpha \approx 3N$ depicted in figure 6(*a*), these results are compelling evidence of the existence of longitudinal LMs. The fuzziness of the obtained values of the reported quantities also led us to suppose that the mixing between modes is strong. Up to this point we can affirm that longitudinal LMs do indeed exist, but are more vague than in the 1D LJ gas and with no hydrodynamical character at all. On the other hand, our results on the transverse correlation

function displayed in figure 9, despite their fluctuations, show a tendency that does not allow us to unambiguously classify them as transverse LMs.

The most important result of this paper was presented in figure 10 for $\rho = 0.5$. Besides a much reduced fluctuation in the studied variables, a very defined jump in $k_{\max}$ at $\alpha \approx 100$ is observed. The importance of this fact is that, for the 1D LJ gas, a similar jump was observed, but for a low-density value [20]. In that system this behavior was interpreted in terms of a separation of timescales signaled by a bending in the LS. In contrast, we obtain a sharply defined jump in $k_{\max}$ at a ρ value in which the corresponding LS shows no bending, as can be observed in figure 3. In order to try to understand this seemingly puzzling result, we have to remember that, from the suspected importance of hyperbolicity for the appearance of the LMs [14], the main results for the 1D LJ fluid were obtained in a relatively diluted regime [20], which made this system somewhat similar to hard-core systems previously studied [48]. However, for $\rho = 0.5$ our system is far from complete hyperbolicity, since the combination of attractive and repulsive interactions induces strong correlations between the collision events that makes it difficult to separate them from each other. At the same time, the aforementioned density value is not high enough to make the effective interaction among atoms similar to that of a lattice of anharmonic oscillators in which hydrodynamic LMs have been detected [25]. Thus there is no obvious mechanism that could account for the sharp jump in $k_{\max}$ when there is no bending in the LS. Therefore the role of the alleged separation of timescales, inferred from the LS bending for the 1D LJ gas, seems to bear no relation to the appearance and phenomenological description of the LMs in our 3D LJ fluid.

6. Conclusion

In this paper we have performed a study of the tangent-space dynamics of the 3D LJ fluid in order to investigate the possible existence of the LMs which are a distinctive feature of the hard-core systems. Our results indicate that longitudinal modes indeed exist for low and high reduced density values, and no conclusive evidence of transverse modes for either density is studied. The lack of a dispersion relation between the LEs and the maximum wave number makes both types of modes markedly different from those already encountered in other systems. The longitudinal LMs turn out to be much better defined for high values of the reduced density. Previously only in hyperbolic systems could LMs be detected at high density values [48]. It is highly plausible that by changing the thermodynamic state of the system the LMs could present a different behavior than that reported in the present paper.

Acknowledgments

One of the authors (M R B) wishes to acknowledge Karen Laurito and D Castañeda-Valle for their comments and suggestions. Financial support from Consejo Nacional de Ciencia y Tecnología (CONACyT) is also acknowledged.

Appendix. Dynamical LV correlation functions

From the Fourier transform of the spatial LV density $\mathbf{u}^{(\alpha)}(\mathbf{r}, t)$, equation (5), we can define the *intermediate two-time correlation function* as

$$\mathcal{F}^{(\alpha)}(\mathbf{k}, \tau) \equiv \langle \widetilde{\mathbf{u}}^{(\alpha)}(\mathbf{k}, t+\tau)\widetilde{\mathbf{u}}^{(\alpha)}(-\mathbf{k}, t)\rangle_t, \tag{A.1}$$

which in the 3D case is a second-rank tensor with components $F^{(\alpha)}_{\mu\nu}(\mathbf{k}, \tau)$. Since the results of section 4.3 point clearly to the existence of longitudinal LMs, we will concentrate

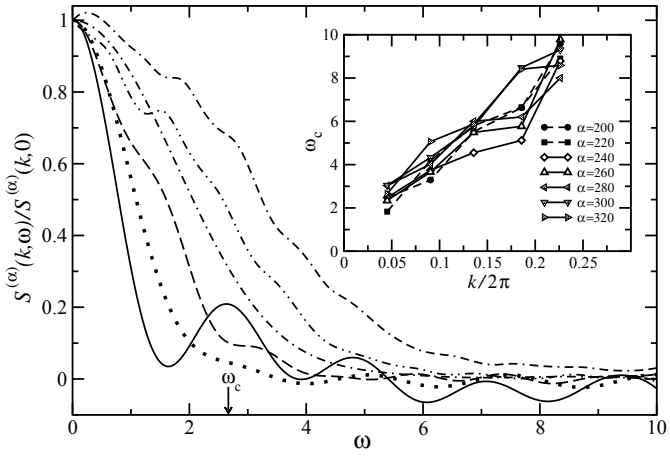

Figure 12. Normalized DLVDCF corresponding to the LV $\alpha = 320$, with $\rho = 0.01, T = 1.5$ and $N = 108$. The curves present results for various values of $k = 2\pi n/L, n = 1, \ldots, 6$ from bottom to top. The arrow indicates the position ω_c of the first peak $n = 1$. The inset displays the dispersion relation $\omega^{(\alpha)}(k)$ for different LVs.

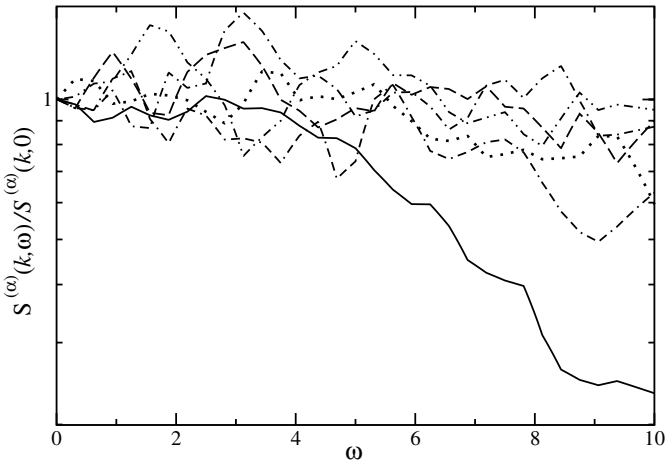

Figure 13. Normalized DLVDCF corresponding to $\alpha = 320$, but for $\rho = 0.5$. Same T and N values as in figure 12.

on the longitudinal component of this function. By following the same methodology of section 4.1 we are led to an expression for the longitudinal component of the form $F_L^{(\alpha)}(k_z, \tau) = \langle \widetilde{u}_z^{(\alpha)}(k_z, t+\tau)\widetilde{u}_z^{(\alpha)}(-k_z, t)\rangle_t$. Taking **k** parallel to the other coordinate directions and averaging we obtain the final form $F_L^{(\alpha)}(k, \tau)$. For $\tau = 0$ we recover the time average of the static LV correlation function, i.e. $\langle C_L^{(\alpha)}(k, t)\rangle_t = F_L^{(\alpha)}(k, \tau = 0)$. The dynamical LV correlation function encodes structural as well as temporal correlations, and thus provides more detailed information of the system.

By Fourier transformation with respect to time we obtain the *dynamical LV density correlation function* (DLVDCF) as $S^{(\alpha)}(k, \omega) = (2\pi)^{-1} \int F_L^{(\alpha)}(k, \tau) \exp(\mathrm{i}\omega\tau)\, \mathrm{d}\tau$. In figure 12 we present the result for $\rho = 0.01$ and $\alpha = 320$ for the longitudinal DLVCF at various integer

multiples of the wave vector $k = 2\pi/L$. It can be observed that, besides the central peak, smaller peaks are present as the frequency ω increases. This result implies that the tangent-space dynamics is described by a set of characteristic frequencies, which may have their origin in the lack of timescale separation already advanced in section 3. However, restricting our attention to the lowest frequencies, it is clear that the position ω_c of the first peak can be unambiguously defined for the lowest k value; a similar identification can be made for other low k values. Thus a dispersion relation $\omega^{(\alpha)}(k)$ for different α values can be extracted. The result is presented in the inset of the same figure. It is observed that an approximately linear dispersion relation is obtained and thus, besides the characteristic wave vector $k^{(\alpha)}$ for each LM already determined in section 4.3, each mode can also be characterized by a frequency $\omega_c(k^{(\alpha)})$. The non-vanishing value of $\mathrm{d}\omega/\mathrm{d}k$ seems to imply propagating wave-like excitations.

The result for the longitudinal DLVDCF at $\rho = 0.5$ is presented in figure 13. In sharp contrast to the low-density state no structure can be observed whatsoever at any wave vector number. No characteristic frequency can easily be identified, which implies that no propagation of any wave-like structures occurs at any wave vector number. Thus the tangent-space structure described in figure 10 remains unaltered within the timescales studied. More details of the temporal dynamics in tangent space will be presented in a forthcoming study.

References

[1] Butera P and Caravati G 1987 *Phys. Rev.* A **36** 962
[2] Torcini A and Antoni M 1999 *Phys. Rev.* E **59** 2746
[3] Firpo M-C 1998 *Phys. Rev.* E **57** 6599
[4] Romero-Bastida M and Braun E 2002 *Phys. Rev.* E **65** 036228
Romero-Bastida M 2004 *Phys. Rev.* E **69** 056204
[5] Evans D J, Cohen E G D and Morriss G P 1990 *Phys. Rev.* A **42** 5990
[6] Barnett D M, Tajima T, Nishihara K, Ueshima Y and Furukawa H 1996 *Phys. Rev. Lett.* **76** 1812
Ueshima Y, Nishihara K, Barnett D M, Tajima T and Furukawa H 1997 *Phys. Rev.* E **55** 3439
Barnett D M and Tajima T 1996 *Phys. Rev.* E **54** 6084
[7] Torcini A, Dellago C and Posch H A 1999 *Phys. Rev. Lett.* **83** 2676
[8] Barnett D M, Tajima T and Ueshima Y 1999 *Phys. Rev. Lett.* **83** 2677
[9] Evans D J and Morriss G P 1990 *Statistical Mechanics of Non-equilibrium Liquids* (New York: Academic)
[10] Gaspard P 1999 *Chaos, Scattering, and Statistical Mechanics* (Cambridge: Cambridge University Press)
[11] Dorfman J R 1999 *An Introduction to Chaos in Nonequilibrium Statistical Mechanics* (Cambridge: Cambridge University Press)
[12] Milanović Lj, Posch H A and Hoover Wm H 1998 *Mol. Phys.* **95** 281
[13] Posch H A and Hirschl R 2000 Simulation of billiards and of hard body fluids *Hard Ball Systems and the Lorentz Gas* ed D Szàsz (Berlin: Springer) pp 279–314
[14] Eckmann J-P and Gat O 2000 *J. Stat. Phys.* **98** 775
[15] Taniguchi T and Morriss G P 2002 *Phys. Rev.* E **65** 056202
[16] Taniguchi T, Dettmann C P and Morriss G P 2002 *J. Stat. Phys.* **109** 747
[17] McNamara S and Mareschal M 2001 *Phys. Rev.* E **64** 051103
Mareschal M and McNamara S 2004 *Physica* D **187** 311
[18] de Wijn A S and van Beijeren H 2004 *Phys. Rev.* E **70** 016207
[19] Hoover Wm G, Posch H A, Forster Ch, Dellago C and Zhou M 2002 *J. Stat. Phys.* **109** 765
[20] Yang H L and Radons G 2005 *Phys. Rev.* E **71** 036211
[21] Forster Ch and Posch H A 2005 *New J. Phys.* **7** 32
[22] Yang H L and Radons G 2006 *Phys. Rev. Lett.* **96** 074101
[23] Yang H L and Radons G 2006 *Phys. Rev.* E **73** 016202
[24] Yang H L and Radons G 2006 *Phys. Rev.* E **73** 016208
[25] Yang H L and Radons G 2006 *Phys. Rev.* E **73** 066201
[26] Allen M P and Tildesley D J 1987 *Computer Simulations of Liquids* (Oxford: Oxford University Press)
[27] Stoddard S D and Ford J 1973 *Phys. Rev.* A **8** 1504

[28] Smit B 1992 *J. Chem. Phys.* **96** 8639
[29] Oseledec V I 1968 *Trans. Moscow Math. Soc.* **19** 197
[30] Benettin G, Galgani L and Strelcyn J M 1976 *Phys. Rev.* A **14** 2338
[31] Shimada I and Nagashima T 1979 *Prog. Theor. Phys.* **61** 1605
[32] Johnson R A, Palmer K J and Sell G R 1987 *SIAM J. Math. Anal.* **18** 1
[33] Goldhirsch I, Sulem P L and Orszag S A 1987 *Physica* D **27** 311
[34] Ershov S V and Potapov A B 1998 *Physica* D **118** 167
[35] Szendro I G, Pazó D, Rodríguez M A and López J M 2007 *Phys. Rev.* E **76** 025202
[36] Ginelli F *et al* 2007 *Phys. Rev. Lett.* **99** 130601
[37] Eckmann J-P and Ruelle D 1985 *Rev. Mod. Phys.* **57** 617
[38] Yang H L and Radons G 2007 *Phys. Rev. Lett.* **96** 164101
[39] Yang H L and Radons G 2008 *Phys. Rev.* E **77** 016203
[40] Dettmann C P and Morriss G P 1996 *Phys. Rev.* E **53** R5545
[41] Ruelle D 1999 *J. Stat. Phys.* **95** 393
[42] Taniguchi T and Morriss G P 2003 *Phys. Rev.* E **68** 046203
[43] Boon J P and Yip S 1991 *Molecular Hydrodynamics* (New York: Dover)
[44] Radons G and Yang H L 2004 *Preprint* nlin.CD/0404028
[45] Berne B J and Pecora R 2000 *Dynamic Light Scattering* (New York: Dover)
[46] Press W H, Teukolsky S A, Vetterling W T and Flannery B P 1992 *Numerical Recipes in Fortran 77* (Cambridge: Cambridge University Press)
[47] Livi R, Pettini M, Ruffo S, Sparpaglione M and Vulpiani A 1985 *Phys. Rev.* A **31** 1039
[48] Forster C, Hirschl R, Posch H A and Hoover Wm H 2004 *Physica* D **187** 294